Langmuir

Article

pubs.acs.org/Langmuir

Growth of Epitaxial $Pt_{1-x}Pb_x$ Alloys by Surface Limited Redox Replacement and Study of Their Adsorption Properties

M. P. Mercer,[†,‡] D. Plana,[§] D. J. Fermín,[†,§] D. Morgan,[∥] and N. Vasiljevic*[,†,‡]

[†]Bristol Centre for Functional Nanomaterials, University of Bristol, Bristol BS8 1FD, U.K.

[‡]School of Physics, H.H. Wills Physics Laboratory, University of Bristol, Bristol BS8 1TL, U.K.

[§]School of Chemistry, University of Bristol, Cantock's Close, Bristol BS8 1TS, U.K.

[∥]Cardiff Catalysis Institute, School of Chemistry, Cardiff University, Cardiff CF10 3AT, U.K.

ABSTRACT: The surface limited redox replacement (SLRR) method has been used to design two-dimensional Pt−Pb nanoalloys with controlled thickness, composition, and structure. The electrochemical behavior of these alloys has been systematically studied as a function of alloy composition. A single-cell, two-step SLRR protocol based on the galvanic replacement of underpotentially deposited monolayers of Pb with Pt was used to grow epitaxial $Pt_{1-x}Pb_x$ ($x < 0.1$) alloys of up to 10 ML thickness on Au substrates. It is shown that by varying the terminating potential of the galvanic replacement step, the Pb atomic content can be controlled in the films. Electrochemical analysis of the alloys showed that the adsorption of both H and CO exhibits similar, and systematic, decreases with small increases in the Pb content. These measurements, commonly used in electrocatalysis for the determination of active surface areas of Pt, suggested area values much lower than those expected based on the net Pt composition in the alloy as measured by XPS. These results show that Pb has a strong screening effect on the adsorption of both H and CO. Moreover, changes in alloy composition result in a negative shift in the potential of the peaks of CO oxidation that scales with the increase of Pb content. The results suggest electronic and bifunctional effects of incorporated Pb on the electrochemical behavior of Pt. The study illustrates the potential of the SLRR methodology, which could be employed in the design of 2-dimensional bimetallic Pt nanoalloys for fundamental studies of electrocatalytic behavior in fuel cell reactions dependent on the nature of alloying metal and its composition.

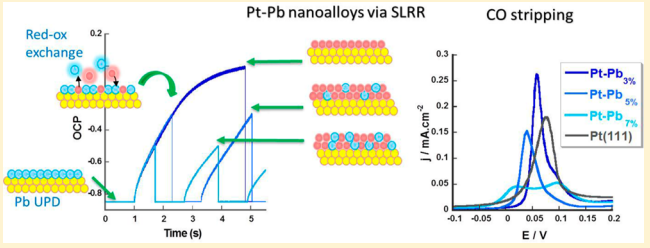

INTRODUCTION

The development of inexpensive, active, and stable Pt catalysts relevant to fuel cell applications remains a very active area of research. While being widely regarded as the most active monometallic catalyst, the susceptibility of platinum to poisoning by CO is recognized as a significant obstacle to its exploitation in fuel cells. Furthermore, the cost of the platinum catalyst is particularly prohibitive to the commercialization of fuel cells. As a result, bimetallic Pt systems have been studied, which possess the simultaneous advantage of a reduction in the required amount of platinum as well as an enhanced catalytic efficiency.[1] In these systems, surface morphology,[2] spatial variation in chemical composition,[3] particle size,[4] and stability[5] are all important and interrelated variables that determine catalytic performance. Substantial progress has been made toward understanding the effect of these factors. However, further work in this area is required to bring this understanding to a level such that a catalyst can be systematically designed for a particular application.[1]

The most promising approaches to improve the performance of Pt catalysts while reducing the total noble metal content include Pt thin-film overlayers[6] and Pt-X alloy skin and skeleton structures that comprise a Pt-rich surface supported on a Pt−X alloy.[3,7] The confinement of the dimensions to a few atomic layers, coupled with the neighborhood of Pt to another metal, causes ligand (electronic) and/or ensemble (geometric) effects that substantially alter the catalytic performance and adsorption binding energies.[8] The primary origin of this effect has been identified as a shift in the position of the d-band of platinum atoms at the surface owing to electron transfer from the surrounding elements. In fact, such a shift has been shown theoretically[9] to affect the binding energy of CO to Pt. However, it is practically difficult to form epitaxial 2-dimensional structures of Pt on a well-defined substrate owing to the very high surface free energy of Pt, which is of the order of 2000 mJ m^{-2},[10] a value much higher than 1400 mJ m^{-2} for Au and 540 mJ m^{-2} for Pb and also due to the low diffusivity of Pt (10^{-16}−10^{-21} cm^2 s^{-1}).[11] Thus, conventional electrodeposition,[12] as well as ultrahigh-vacuum (UHV)-based deposition techniques,[13] usually results in preferential nucleation of Pt at defect sites and a Volmer−Weber growth mode.

In order to overcome the problem of nonuniform Pt growth, Brankovic et al. introduced a new method called surface limited redox replacement (SLRR).[14] In this method, epitaxial growth

Received: June 26, 2015
Revised: August 17, 2015
Published: September 15, 2015

DOI: 10.1021/acs.langmuir.5b02351
Langmuir 2015, 31, 10904−10912

of Pt was obtained using underpotential deposition (UPD) of a less noble sacrificial metal, such as Cu, followed by galvanic replacement by Pt^{4+} from $PtCl_6^{2-}$ in solution.[14] Such Cu UPD-based SLRR protocols resulted in Pt monolayer catalysts with high activity and stability.[15] The Cu UPD-based SLRR protocol has been adopted by many groups as a method for the growth of Pt films of different thicknesses (>1 ML).[16] Most recently, it has been demonstrated that using Pb UPD as a sacrificial layer produces higher quality Pt films than those grown by Cu UPD.[17] In this work, K_2PtCl_4 was used as the source of Pt in a single cell resulting in epitaxial growth and negligible roughness evolution in the electrodeposited films, for film thicknesses of up to 10 ML. Moreover, for the first time this work examined and showed a small extent of sacrificial metal incorporation, which is an aspect of relevance but often neglected in the analysis of SLRR grown films.

The growth of monolayer thick bimetallic alloy catalysts $Pt_{0.8}M_{0.2}$ (M = Au, Pd, Ir, Ru, Rh, Re, or Os) using the SLRR of Cu UPD[18] has been shown by Vukmirovic et al. The study also showed an enhancement of the oxygen reduction reaction on the deposited alloys, but very little attention was given to the fundamental aspects of SLRR methodology and the optimization of growth parameters. The only systematic formation of Pt_4Cu intermetallic thin film of controlled single crystal structure by the SLRR of Pb UPD by both Pt^{2+} and Cu^{2+} ions has been demonstrated recently by Bromberg et al.[19] The stoichiometry of the intermetallic Pt_4Cu films was attained by utilizing 4:1 proportion of Pt^{2+} and Cu^{2+} ions in solution. There has not been much done in terms of using SLRR for random alloy films formation over a range of different compositions. In a work by Fayette et al.,[17] a SLRR protocol for deliberately incorporating sacrificial UPD Pb in films grown by 300 replacements of Pb UPD by $PtCl_4^{2-}$ was demonstrated on a proof-of-concept level. This study showed that $Pt_{1-x}Pb_x$ alloys of varied Pb composition could be formed by decreasing the potential at which the SLRR replacement was interrupted. However, the application of this approach to the controlled epitaxial formation of ultrathin Pt_xPb_{1-x} films has not yet been carried out.

Pt−Pb is an interesting bimetallic system, owing to the reported promoting catalytic effects by the presence of Pb. More specifically, the current density of the formic acid oxidation reaction has been shown to be enhanced by Pb UPD on polycrystalline Pt[20] and Pt single crystals.[21] In the work of Hwang et al., films of Pt_xPb_{1-x} alloys of 6−10 nm in thickness were grown by underpotential codeposition of Pb with Pt.[22] The composition was varied by controlling the potential of deposition. The formic acid oxidation activity was shown to be enhanced by incorporated Pb.[22] In addition, intermetallic PtPb crystals formed by arc melting and sintering treatment have shown high CO tolerance[23] and activity for the electrooxidation of small organic molecules.[24] Pt_3Pb and Pt_3Pb−Pt core−shell nanoparticles have shown to be highly active for the oxidation of formic acid as well.[25] While these studies demonstrate the potential of Pb to enhance the electrocatalytic activity of Pt, a quantitative explanation of the effect of Pb as well as a separation of additional effects from particle size and structure is presently lacking.

The aim of the present work is to demonstrate the applicability of the SLRR technique for the growth of epitaxial ultrathin $Pt_{1-x}Pb_x$ films with controlled thickness, structure, and alloy composition. Furthermore, we examined the effect of low Pb content in the $Pt_{1-x}Pb_x$ alloys on the electrochemical adsorption of H and CO, both of which are commonly used to measure the electrochemically active surface area (ECSA) in Pt systems. The initial part of the work demonstrates the optimization of the SLRR protocol and selection of potentials within Pb UPD region to grow epitaxial alloy films of varied composition. Thin films of differing Pb content were characterized by X-ray photoemission spectroscopy (XPS) to determine their compositions. The electrochemical behavior of the alloys has been characterized by H UPD and CO stripping and solution oxidation with the goal to elucidate the role of Pb in these electrochemical adsorption processes.

EXPERIMENTAL SECTION

Sulfuric acid (Alfa Aesar, 99.9999%), perchloric acid (Aldrich, 99.999%), sodium perchlorate hydrate (Aldrich, 99.99%), puratronic lead(II) carbonate (Alfa Aesar, 99.999%), and potassium tetrachloroplatinate (Aldrich, 99.99%) were used within this work. All solutions were made with Millipore Milli-Q water. The solutions were deoxygenated by Ar (Pureshield argon, 99.998%, BOC) for at least 30 min prior to measurements. A blanket of Ar gas was maintained above the cell during measurements. A mercury/mercurous sulfate (MSE) electrode in saturated K_2SO_4 was used as a reference electrode, and Pt wire was used as a counter electrode in all measurements. All potentials, unless stated otherwise, will be reported with respect to MSE. The electrochemical measurements and the control of electrodeposition were performed using a CompactStat (Ivium Technology) potentiostat.

Substrates. Au thin films of 150 nm thickness evaporated under high vacuum onto Schott Nexterion glass slides with a 10 nm Ti adhesion layer were used as substrates to grow $Pt_{1-x}Pb_x$ alloys.[17] Prior to the electrochemical experiments, the Au surface was flame annealed in a Pyrex tube for 5 min under ultrapure nitrogen flow. The electrochemically active surface area (ECSA) of Au was obtained by integration of the surface oxide reduction peak (assuming a charge of 440 $\mu C\ cm^{-2}$ per ML) measured by cyclic voltammetry in 0.5 M H_2SO_4 solution, in a potential range of 0.0−0.95 V.[26] The measured ECSA of Au was used as the geometric area of the sample, and all current values throughout the paper were normalized to this value.

A polycrystalline Pt (Pt-poly) rod, of diameter 2 mm, embedded in poly(ether ether ketone) (PEEK), was prepared by successive mechanical polishing using alumina suspensions (Buehler) from 1.0 μm to 0.3 μm down to 0.05 μm particle size. The surface was introduced to the electrochemical cell in a hanging meniscus configuration and subjected to electrochemical activation by at least 20 cyclic voltammetry scans in 0.5 M H_2SO_4 in the potential window −0.66 to 0.70 V at ν = 50 mV s^{-1}. A Pt(111) single crystal (0.5° miscut) of 10 mm diameter and 3.0 mm thickness (Metal Crystals and Oxides Ltd.) was mechanically polished with 0.05 μm alumina suspension (Buehler) until a shiny mirror finish was obtained. Prior to experiments, the crystal was cleaned and annealed for 10 min in a butane−propane flame to an orange color. The crystal was then left to cool in an ultrapure nitrogen stream, protected by a 0.5 M H_2SO_4 droplet, and transferred to a cell containing 0.5 M H_2SO_4 solution in a hanging meniscus configuration. For all measurements on Pt-poly and Pt(111) current values were normalized with respect to the ECSA obtained from underpotentially deposited hydrogen (H UPD), under the assumption of a charge per unit area of 210 $\mu C\ cm^{-2}$ for the H UPD layer.[27]

SLRR Deposition Protocol. SLRR deposition was carried out in a single-cell containing solution 10^{-1} M $NaClO_4$ + 10^{-3} M $HClO_4$ + 10^{-3} M $Pb(ClO_4)_2$ + 5×10^{-4} M K_2PtCl_4 following a protocol similar to the one previously described.[17] The Pb UPD layer was formed by application of potential step at E_1 = −0.85 V for 1 s, after which the potential control was interrupted and the open circuit potential (OCP) was monitored as the galvanic replacement of Pb UPD by Pt^{2+} proceeded. The galvanic replacement reaction was interrupted when the OCP reached a selected positive potential limit, E_2, at which a potential pulse to E_1 was applied and another SLRR deposition cycle

DOI: 10.1021/acs.langmuir.5b02351
Langmuir 2015, 31, 10904−10912

was triggered. All $Pt_{1-x}Pb_x$ alloys were formed using 10 SLRR deposition cycles. After the SLRR growth, the electrode was rinsed with Millipore Milli-Q water and transferred to an electrochemical cell containing 0.5 M H_2SO_4 and subjected to cyclic voltammetry (CV) between −0.66 and 0.40 V at ν = 50 mV s^{-1}. Potential cycling resulted in a stable and representative behavior, i.e., H UPD, which generally was obtained after five CV cycles. Small changes of CVs during initial scans did not show additional peaks that would suggest dealloying or redeposition/dissolution of Pb in the underpotential regime. For the sake of consistency all samples in this work were subjected to 15 CV cycles in 0.5 M H_2SO_4. After representative H UPD voltammetry was recorded, the samples were subjected to further electrochemical or XPS measurements.

CO Electro-Oxidation Experiments. After confirmation of a stable surface behavior by H UPD, CO (research grade purity N3.7, BOC) was inserted into the cell for at least 10 min while polarizing the electrode at −0.60 V. Five scans were performed at 20 mV s^{-1}, sweeping anodically from −0.60 V up to 0.70 V in the CO-saturated solution. Cyclic voltammetry was then performed after purging the electrolyte for at least 50 min with Ar while maintaining potential control at −0.60 V. The electrode was then swept anodically up to 0.70 V at 20 mV s^{-1}, and CV was performed until a stable H UPD voltammogram was obtained. The first cycle was CO stripping voltammetry; the second one confirmed the absence of residual CO in solution.

XPS Measurements. A Kratos Axis Ultra DLD system was used to collect XPS spectra using a monochromatic Al Kα X-ray source operating at 144 W. The data were collected with pass energies of 160 eV for survey spectra and 40 eV for the high resolution scans. The system was operated in the Hybrid mode, using a combination of magnetic immersion and electrostatic lenses and acquired over an area approximately 300 × 700 μm^2. A magnetically confined charge compensation system was used to minimize charging of the sample surface, and all spectra were taken with a 90° takeoff angle. A base pressure of ~1 × 10^{-9} Torr was maintained during collection of the spectra. All XPS spectra were collected following the deposition of $Pt_{1-x}Pb_x$ films by SLRR and the subsequent characterization of the films by H UPD as described above.

RESULTS AND DISCUSSION

Growth of $Pt_{1-x}Pb_x$ Films by SLRR. The selection of the SLRR potential limits for the growth of alloys can be best illustrated by examining Pb UPD on Au and Pt, shown by cyclic voltammograms in Figure 1. Pb UPD was conducted in the Pt-free solution, 10^{-1} M $NaClO_4$ + 10^{-3} M $HClO_4$ + 10^{-3} M $Pb(ClO_4)_2$, at ν = 50 mV s^{-1}. On both Au substrates and Pt films the UPD layer is fully formed in the region between −0.75 and −0.85 V, and the characteristic UPD features serve as indicators of good substrates quality. Figure 1 shows the representative characteristics of Pb UPD on a well-defined Au(111) surface,[28] such as the splitting of the main UPD peak, specific to the energetically separated processes of deposition/dissolution on terraces and steps, as well as the surface dealloying peak at −0.2 V.[29] Pb UPD on Pt film grown on Au substrates using 10 SLRR deposition cycles under the conditions described by Fayette et al.[17] is also shown in Figure 1. Such deposited Pt films have been shown to exhibit a pronounced (111) texture, as confirmed by XRD. These films are characterized by small Pt domains of 5−10 nm size which follow the morphology of the Au substrate (i.e., quasi-2D growth).[17] It can be clearly observed that Pb UPD on Pt is characterized by a single main peak at 0.0 V, followed by an almost featureless region in the range of −0.85 to −0.40 V. At potentials more positive than 0.0 V, the features from Pb UPD are convoluted with those from OH_{ads}; first, this process takes place in the potential region of OH_{ad} adsorption on Pt in perchlorate solution, and second, the previous rotating ring disk electrode work by Grgur et al.[30] has shown that the partially formed Pb UPD layer stabilizes the formation of OH_{ad} species, shifting its adsorption to more negative potentials. Because of a partial overlap of the features associated with the desorption of Pb adatoms and the adsorption of OH_{ads} on Pt(111),[30] the potential window was varied in attempt to more clearly distinguish the relative contributions. In general, the UPD voltammetry has the main characteristics of a Pt(111) surface, as indicated by a small peak observed at approximately −0.15 V and a shoulder close to −0.05 V, indicating the presence of (111) domains.[31] The notable difference is the absence of pronounced reversible peaks (i.e., Pb monolayer densification and phase transformation peaks) in the potential range negative of the main peak, which is a consequence of the small domain size of the electrodeposited Pt.[17]

An examination of the Pb UPD features is relevant for the selection of the potential limits, E_1 and E_2, which were monitored and used to maintain control of Pt deposition during the SLRR protocol. The schematic of the protocol is presented in Figure 2. For the growth of Pt films in the single-cell SLRR method, as previously described,[17] E_1 was the potential at which the UPD layer was formed. It can be seen from Figure 1 that the selected value of E_1 = −0.85 V was sufficiently negative to maximize the Pb UPD coverage on both the Au and the Pt substrates. Based on our previous work, a pulse of 1 is long

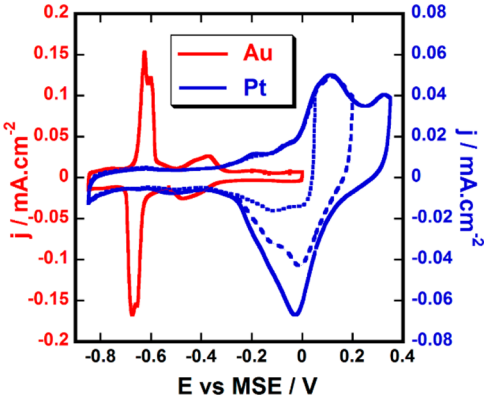

Figure 1. Cyclic voltammograms of Pb UPD on Au and Pt surfaces in 10^{-1} M $NaClO_4$ + 10^{-3} M $HClO_4$ + 10^{-3} M $Pb(ClO_4)_2$ at a scan rate of 50 mV s^{-1}.

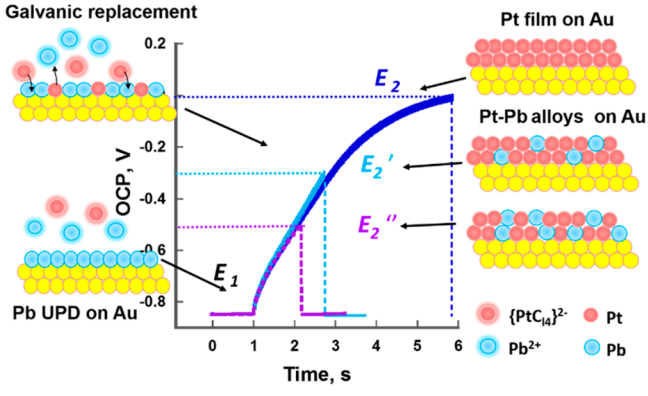

Figure 2. Schematic presentation of the SLRR protocol used to electrodeposit $Pt_{1-x}Pb_x$ alloys. Different alloy compositions are formed by changing the potential limit E_2 of OCP step termination.

DOI: 10.1021/acs.langmuir.5b02351
Langmuir 2015, 31, 10904−10912

enough for the Pb UPD layer to complete (in less than 0.5 s), yet not too long to allow significant Pt coelectrodeposition to take place in a so-called surfactant growth regime.[32] Previously reported measurements using a quartz crystal microbalance showed about 1% of additional Pt deposited compared to what would be expected by galvanic replacement of the Pb UPD layer alone.[17] During the second step of the SLRR cycle, the OCP was monitored during the replacement of the Pb UPD layer with Pt. Once the OCP reached the value E_2 = 0.0 V, corresponding to a Pb-free surface on Pt and Au, a potential step back to E_1 was triggered.

In the present work we created $Pt_{1-x}Pb_x$ alloys by performing 10 SLRR cycles with different E_2 potentials, selected between 0.0 and −0.50 V. The films grown at E_2 = 0.0 V were chosen in this work as the suitable point for comparison for all $Pt_{1-x}Pb_x$ alloy films grown at lower potentials E_2, as they have been shown to exhibit typical "pure"-Pt electrochemical behavior.[17] For each alloy, the galvanic replacement was interrupted at a potential E_2 with partial monolayer amount of Pb still present on the surface, as shown in Figure 2. The amount of the replaced and the remaining Pb on the surface at the selected E_2 value could be theoretically estimated from the Pb adsorption isotherm. However, the stabilization of OH_{ad} and the overlap with Pb UPD in the selected region of the potentials in stagnant electrolyte make the exact Pb coverage determination difficult.[30] So instead of targeting a particular amount of Pb on the surface, we focused on the selection of the potential limit, over a relatively wide range, below 0.0 V for which SLRR growth was shown to produce almost pure Pt films, i.e., films with smallest amount of incorporated Pb.[17]

The potential and current transients of the SLRR replacements obtained during SLRR growth with different E_2 limits are shown in Figure 3. The transients show that for each selected E_2 growth limit OCP replacement steps were completed within the same time, with the maximum time for samples grown with E_2 = 0.0 V less than 10 s, as already reported.[17] The time interval for each OCP replacement reduces with decreasing values of the selected potential E_2. In addition, the time required for each replacement step did not change significantly after the first replacement, suggesting uniform growth and no significant changes in the kinetics of replacement during successive SLRR cycles.

Surface Characterization: H UPD and XPS. Following the SLRR growth, $Pt_{1-x}Pb_x$ films were subjected to potential cycles and characterization in 0.5 M H_2SO_4, as described in the Experimental Section. The samples were further characterized by XPS to assess the amount of Pb in the alloy, and representative XPS spectra are shown in Figure 4 for illustration. The XPS measured Pb composition of the examined alloys is listed in Table 1. It can be observed that a maximum Pb content achieved by SLRR protocol at E_2 = −0.5 V is of the order of 7%. The SLRR protocol at E_2 = 0.0 V also confirms the previously reported Pb sacrificial layer incorporation of 3.5%.

Representative H UPD behavior of the grown alloys is presented in Figure 5 along with H UPD on Pt(111) for comparison. It can be observed that H UPD on Pt films grown with E_2 = 0.0 V and the integrated charges from H UPD, which are shown in Table 1, are in good agreement with previously obtained results under the same conditions.[17] The characteristic "butterfly" peaks, which are associated with an order/disorder transition in the sulfate adlayer, can be observed on Pt(111), and the "disappearance" of these peaks on the grown films can

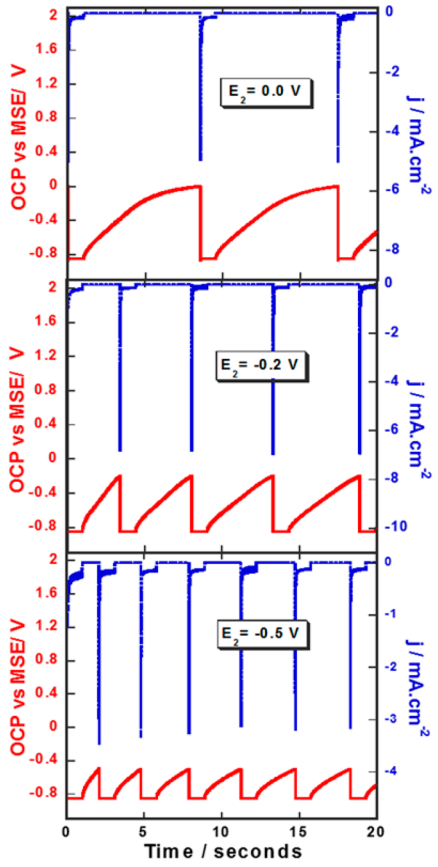

Figure 3. Open circuit potential transients and current recorded during successive SLRR cycles of $Pt_{1-x}Pb_x$ film growth with different values of the E_2 potential: (a) 0.0, (b) −0.2, and (c) −0.5 V. The solution was 10^{-1} M $NaClO_4$ + 10^{-3} M $HClO_4$ + 10^{-3} M $Pb(ClO_4)_2$ + 5×10^{-4} M K_2PtCl_4 with the potential E_1 = −0.85 V for all samples.

be attributed to the very small size, of the order of 5−10 nm of the Pt domains.[31] The films grown at a lower value of E_2 show a systematic decrease in H-UPD charge and the peaks at −0.59 and 0.45 V corresponding to the adsorption on (110) and (100) sites, respectively, suggesting that more Pb is incorporated in the surface. The results thus indicate Pt−Pb alloy formation, and as expected there is a systematic reduction of the H UPD charge owing to the fact that H does not adsorb on Pb.

Under the simple assumption that each extra Pb atom blocks one Pt site for H adsorption, it would be expected that the H UPD charge should decrease in the same proportion as the reduction in Pt content. However, the compositions of alloys as measured by XPS do not confirm this assumption. The integrated charge of the H UPD and the percentage of decrease are listed in Table 1 alongside the corresponding Pb composition measured by XPS. The data presented in Table 1 show significant changes of the H UPD charge with relatively small changes in the alloy composition, much larger than what simple site blocking would predict. The results suggest that Pb might have screening (blocking) effect on neighboring Pt sites for H-adsorption. In fact, similar blocking effects are well-known and reported for UPD processes on surface alloys, namely Pb UPD on Pb−Ag(111)[33] and H-UPD on Ag−Pt(111).[34]

Considering a very simple model, in the limit of low Pb coverages and isolated Pb atoms, it would be expected that the

DOI: 10.1021/acs.langmuir.5b02351
Langmuir 2015, 31, 10904−10912

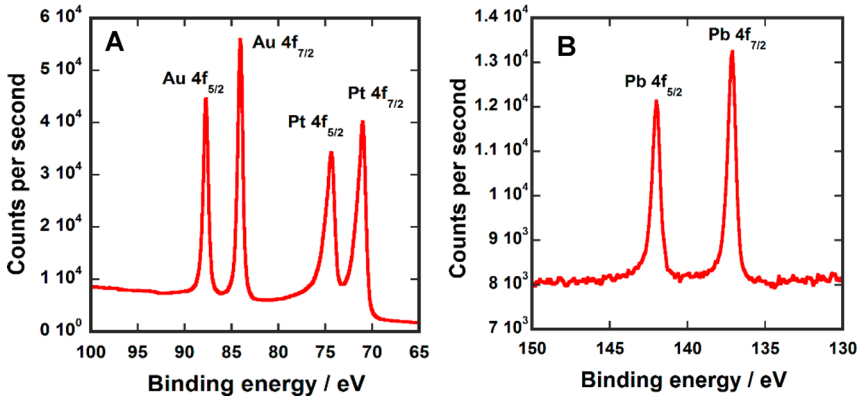

Figure 4. XPS spectra, recorded for a sample grown by 10 SLRR cycles in 10^{-1} M $NaClO_4$ + 10^{-3} M $HClO_4$ + 10^{-3} M $Pb(ClO_4)_2$ + 5×10^{-4} M K_2PtCl_4 solution with E_2 = −0.2 V. (A) Au 4f and Pt 4f peaks; (B) Pb 4f peaks.

Table 1. Comparison of Charges Obtained by H UPD on $Pt_{1-x}Pb_x$ Films with the Atomic Percentages of Pb Obtained by XPS

E_2 (V)	$Q_{H\,UPD}$ (μC cm^{-2})	ΔH UPD (%)	XPS Pb (at. %)
0.0	192 ± 19		3.5
−0.2	169 ± 17	12	5.2
−0.5	140 ± 14	27	6.9

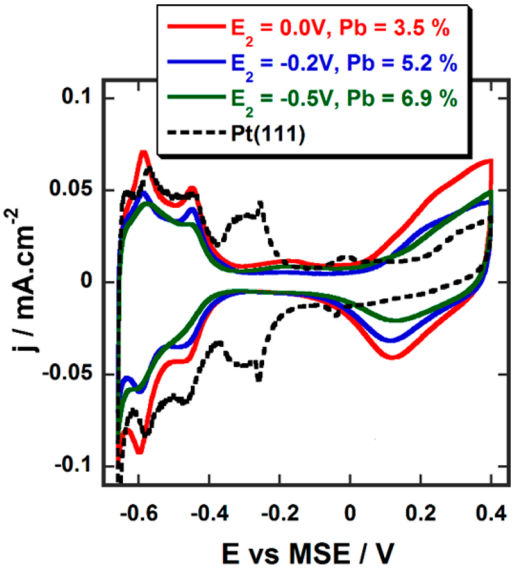

Figure 5. Cyclic voltammograms of H UPD (scan rate 50 mV s^{-1}) in 0.5 M H_2SO_4 on $Pt_{1-x}Pb_x$ films grown by 10 SLRR cycles in 10^{-1} M $NaClO_4$ + 10^{-3} M $HClO_4$ + 10^{-3} M $Pb(ClO_4)_2$ + 5×10^{-4} M K_2PtCl_4 solution using different values of E_2 potential as marked. The atomic percentages of Pb in alloy films associated with different E_2 potentials were measured by XPS.

H UPD charge then decreases with the number of Pb atoms ($\theta_{Pb} = x$) affecting n Pt nearest-neighbor atoms as

$$\theta_{H\,UPD} \sim 1 - k\theta_{Pb} \quad (1)$$

where $\theta_{H\,UPD}$ and θ_{Pb} are the coverage of H UPD and the composition of Pb in the topmost atomic layer, respectively, and $k = n + 1$. By examining Figure 6, it appears that a linear relationship is a suitable interpolation within experimental error. The value of k obtained by a linear fit to the data presented in Figure 5 is 7 ± 1. A value of 7 suggests that each

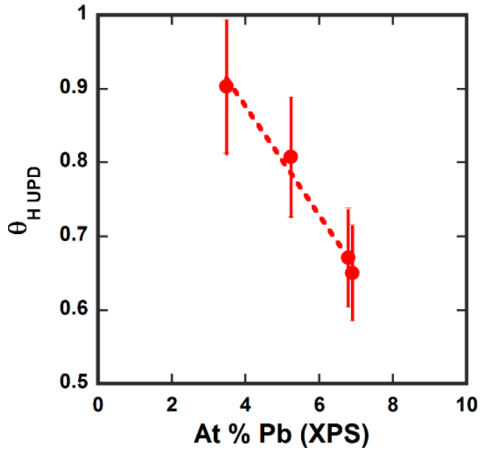

Figure 6. Coverage of H UPD as a function of the atomic percentage of Pb obtained from XPS measurements.

Pb atom blocks six adsorption sites for H adsorption, which is the value that corresponds to the number of nearest neighbors in a Pt(111) surface layer. This result is the same as the one obtained by Popov et al.,[33] who determined that every Pb atom in the Ag−Pb (Pb <10 at. %) surface alloy affects six adsorption sites for subsequent Pb UPD adsorption. Besides, the linear dependence between the H UPD coverage and Pb composition is in agreement with the "percolation cluster model" of underpotential deposition on alloy surfaces.[35] While this analysis is simple and based on the Pb being present in the topmost layer, we cannot exclude a possibility of subsurface Pb atoms affecting adsorption of enriched Pt sites on top. In fact, a similar significantly reduced coverage of H UPD has been observed on $Pt_3Ni(111)$ skin structures.[7] Also, recent work by Brimaud et al.[36] showed that in the Pt_xAu_{1-x}/Pt system the charge obtained by H UPD was in discordance with the amount of Pt at the surface (Figure 3 in ref 36), but the charge was found to decrease nonlinearly with the atomic fraction of Au.[36] In the work by Fayette et al.,[17] the $Pt_{1-x}Pb_x$ alloys showed a higher Pb content for each given E_2 value. This difference, besides an overestimate of the Pb content obtained by EDS measurements compared to that measured by XPS, can be attributed mainly to the much higher thickness of the alloys grown in that work (~30 times) and significant roughness that develops during thicker alloy growth which assists increasingly higher Pb incorporation. The effect of the performing more than 10 SLRR replacements on the composition of the alloys,

DOI: 10.1021/acs.langmuir.5b02351
Langmuir 2015, 31, 10904−10912

as well as the Pb distribution with respect to thickness, will be a matter of separate publication and analysis.

CO Electro-Oxidation. It is known that in certain Pt bimetallic systems the charge obtained by CO stripping is a more reliable measure of surface Pt content than the H UPD charge.[7,37] In particular, on $Pt_3Ni(111)$ skin structures,[7] H UPD was suppressed by subsurface Ni, but the corresponding charge obtained by CO stripping was the same as for Pt(111). This phenomenon is considered to be an effect of the much stronger CO interaction with Pt in comparison with H. To assess whether a similar effect could be observed on deposited $Pt_{1-x}Pb_x$ alloys, CO stripping voltammetry was performed, and the first scans of the electro-oxidation of CO in solution are presented in Figure 7. The charges obtained by integrating the

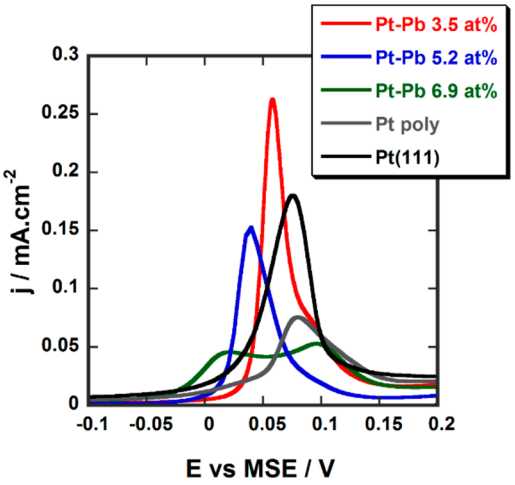

Figure 7. CO stripping on $Pt_{1-x}Pb_x$ films with differing alloy content, performed at a scan rate of 20 mV s^{-1} in 0.5 M H_2SO_4.

stripping peaks, which are presented together with the H UPD charges and XPS results in Table 2, are indistinguishable from

Table 2. Comparison of the Integrated Charge of H UPD and CO Stripping from Pt−Pb Alloys and ΔE_{CO}[a]

E_2 (V)	at. % Pb	$Q_{H\,UPD}$ (μC cm^{-2})	$0.5Q_{CO}$ (μC cm^{-2})	ΔE_{CO} (V)
0	3.5	192 ± 19	197 ± 20	0.02
−0.2	5.2	169 ± 17	153 ± 15	0.04
−0.5	6.9	140 ± 14	135 ± 14	0.06

[a] ΔE_{CO} is the shift in the potential of the first peak of CO oxidation with respect to the value obtained for Pt(111).

those obtained by H UPD, within the error. Therefore, it is likely that the above arguments regarding the screening effect of Pb on H UPD adsorption must also apply to CO.

Although it is somewhat surprising that the coverage of both adsorbates is affected in a similar way by Pb, the effect is not unknown in other bimetallic Pt−X systems: the charges obtained by CO stripping and H UPD were found to be in quantitative agreement on Pt_3Co nanostructures,[38] even though both adsorbates underestimated the true active area of Pt. Clearly, the degree of agreement between H UPD and CO stripping charges in Pt bimetallic systems is dependent on the nature of the system, i.e., alloying metal.

In CO stripping experiments, not only is the charge under the peak meaningful, but so is the onset potential for the oxidation of CO. A more negative onset potential for CO oxidation can indicate a lower energy cost associated with the removal of CO. Alternatively, within the Langmuir−Hinshelwood mechanism of CO oxidation,[39] it can indicate a lower potential for the nucleation of OH_{ads} species that are required for CO stripping. The position of the CO stripping peak of Pt(111), which is centered on 0.072 V, is in agreement with literature values.[40] Similarly, the experimentally obtained position of 0.080 V on polycrystalline Pt agrees with literature values at pH = 0.3.[41] It should be pointed out that the peak position is very sensitive to the presence of defects and steps on the prepared Pt surface. The single crystal surface morphology is dependent on the cooling atmosphere.[42] Cooling the surface in an argon−hydrogen atmosphere rather than air resulted in a difference of 0.09 V in the peak position. This difference was ascribed to a higher incidence of defects on the air-cooled crystal. These defects acted as nucleation centers for the adsorption of OH_{ads}. Similarly, any misorientation of the surface with respect to Pt(111)[43] resulted in a negative shift of the position of the oxidation peak due to the nucleation of OH_{ads} on step edges. From the voltammograms of the single crystal Pt electrode, shown in Figure 5, as well as the obtained values for the CO peak positions, it is apparent that the Pt(111) crystal has a relatively high defect density despite possessing long-range order. Actually, in our case the high defect density of the crystal facilitates a comparison with the SLRR grown films as these are also defect-rich and statistically comparable. A significant negative potential shift in the onset of CO stripping with increasing Pb content is clearly observed. One possible explanation for the shift is that the presence of Pb atoms could cause a reduction in the local potential of zero charge (pzc); this effect has already been observed in the context of Pb UPD on Pt(111) single crystals.[30,44] The potentials of *total zero* free charge (pztc) of Pt surfaces, i.e., the potentials at which the free charge in the double layer is perfectly balanced by the charge from chemisorbed species, have been determined by the CO charge displacement technique[45] and N_2O reduction;[46] the pztc for Pt(111) in 0.5 M H_2SO_4 was found to be 0.28 V vs Pd|H.[46b] For comparison, the pzc of Pb was found to be −0.62 V vs NHE by differential capacitance measurements.[47] Such a difference, even with the low atomic percentages of Pb in the films, could lead to a lower onset for the formation of OH_{ads} species that are required for the removal of adsorbed CO, in a manner similar to the effect that has been described on PtRu[48] and Pt_3Sn[49] alloys.

In addition, two distinct peaks are observed for the most Pb-rich alloy, and a shoulder is observed in the results obtained for the alloys of lower Pb content. The significance of two CO stripping peaks could be explained in terms of the formation of CO islands with a higher local packing density,[43] which correspond to more a more weakly bound state of CO. In fact, such an effect has also been observed on Pt(111) electrodes modified by Ru clusters when the Ru coverage was in the range 0−20 at. %.[50] In that system, the more negative peak was attributed primarily to the removal of CO linearly bonded to Ru while the more positive one was associated with CO linearly bound to Pt, with additional charge on the more negative peak being assigned to the oxidation of CO on Pt sites neighboring Ru. In the present system, such an explanation is unlikely since CO is predicted not to bond to Pb. One possibility is that multiple adsorption sites of differing energy are created by the different coordination of Pb to Pt, so that Pt atoms with more Pb neighbors would bind CO less strongly and so lead to a

DOI: 10.1021/acs.langmuir.5b02351
Langmuir 2015, 31, 10904−10912

coexistence of two surface domains with different CO adsorption energy.

As additional point of comparison, measurements were performed in CO-saturated solution, on surfaces with differing composition. The results are presented in Figure 8. The

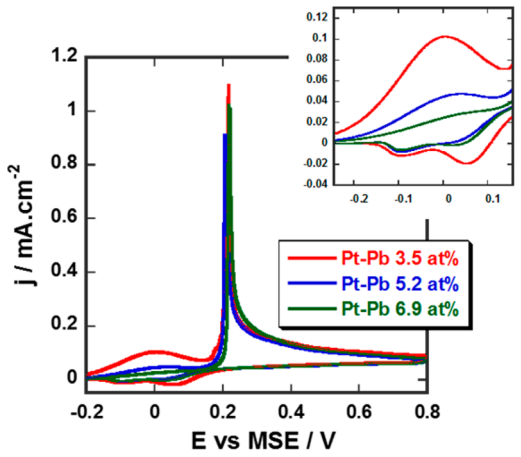

Figure 8. Cyclic voltammetries of $Pt_{1-x}Pb_x$ alloys with different composition in CO-saturated 0.5 M H_2SO_4, scan rate 20 mV s^{-1}.

positive shift in the position of the main peak of CO oxidation with respect to the potential of CO stripping (in CO-free solution) is consistent with the behavior observed on Pt(111) and polycrystalline Pt.[51] However, Figure 8 reveals that the potential of the main peak did not change significantly with the alloy composition, in contrast to the results obtained by CO stripping. This is unexpected result as we are not aware of any other Pt−X alloy system that displays a shift in the CO stripping potential with increasing X composition, without showing a shift in the CO solution oxidation potential. While at present we do not have complete understanding for the observed behavior, it is possible that with CO present in solution the oxidation of CO was not limited by the rate of OH_{ads} adsorption.

Variations are also observed in the CO bulk oxidation at lower overpotentials, namely in the region between −0.2 and 0.2 V, as shown in the inset of Figure 8. The origin of CO oxidation in this so-called "preignition" potential region has been extensively studied on polycrystalline Pt and Pt single crystal electrodes.[51a,52] The CO oxidation, present only during the first potential scans,[2,52] can be associated with Pt sites freed from weakly bonded CO or Pt defects which heal by subsequent potential cycling. The results on $Pt_{1-x}Pb_x$ alloys show a systematic decrease in current density with increasing of the Pb content. This behavior could be due to a lowering of the local CO coverage of weakly bonded CO with increasing Pb composition in the alloy. Again, the full understanding will require further studies on this and other alloy systems.

CONCLUSIONS

In this work, we demonstrated the viability of the one cell SLRR technique involving the replacement of Pb UPD with Pt^{2+} for the growth of $Pt_{1-x}Pb_x$ ultrathin films. By systematically varying the potentials within SLRR, the Pb content in the alloy was controlled. It was shown that for films of the same thickness, i.e., grown by the same number of SLRR cycles, even small changes in the amount of alloyed Pb significantly affected the charges measured by H UPD and CO stripping. The charge values obtained by these methods were in agreement, within experimental uncertainty. The magnitude of the change in adsorbate coverage with increasing Pb content is much greater than that expected purely from the substitution of Pt for Pb in the uppermost atomic layer, possibly due to electronic effects induced by Pb. A different trend in the position of the peak of CO oxidation in CO-free and CO-saturated solutions was obtained, and some changes in peak shape were observed. This observation may be due to a bifunctional effect in which Pb provides oxygenated species at an earlier onset potential. Two well-separated peaks were observed for the most Pb-rich films, which may have been a consequence of domains of different CO packing density on regions of the surface with differing Pb content.

The comparison and analysis of H and CO adsorption have important implications for the fundamental understanding of the effects of alloying and film thickness on electrochemical adsorption and catalytic performance in Pt alloy nanostructures. The effect of controlling film thickness and Pb content on the electro-oxidation of formic acid in the context of the work presented here, as well as a full discussion of the variation of composition with depth, will be the topic of a future publication.

AUTHOR INFORMATION

Corresponding Author

*E-mail n.vasiljevic@bristol.ac.uk; Ph +44 (0) 117 331 7739; Fax + 44 (0) 117 925 5624 (N.V.).

Notes

The authors declare no competing financial interest.

ACKNOWLEDGMENTS

The authors of this work acknowledge the financial support of the UK Engineering and Physical Sciences Research Council (EPSRC) as part of grant code EP/G036780/1. M.P.M, N.V., and D.J.F. acknowledge the support of the Bristol Centre for Nanoscience and Quantum Information, University of Bristol. We are grateful to Dr. Neil A. Fox, School of Physics University of Bristol, for the ultrahigh vacuum deposition of Au films on glass.

REFERENCES

(1) Debe, M. K. Electrocatalyst approaches and challenges for automotive fuel cells. *Nature* **2012**, *486*, 43−51.

(2) Strmcnik, D. S.; Tripkovic, D. V.; van der Vliet, D.; Chang, K.-C.; Komanicky, V.; You, H.; Karapetrov, G.; Greeley, J. P.; Stamenkovic, V. R.; Markovic, N. M. Unique Activity of Platinum Adislands in the CO Electrooxidation Reaction. *J. Am. Chem. Soc.* **2008**, *130*, 15332−15339.

(3) Stamenkovic, V. R.; Mun, B. S.; Mayrhofer, K. J. J.; Ross, P. N.; Markovic, N. M. Effect of Surface Composition on Electronic Structure, Stability, and Electrocatalytic Properties of Pt-Transition Metal Alloys: Pt-Skin versus Pt-Skeleton Surfaces. *J. Am. Chem. Soc.* **2006**, *128*, 8813−8819.

(4) Arenz, M.; Mayrhofer, K. J. J.; Stamenkovic, V.; Blizanac, B. B.; Tomoyuki, T.; Ross, P. N.; Markovic, N. M. The Effect of the Particle Size on the Kinetics of CO Electrooxidation on High Surface Area Pt Catalysts. *J. Am. Chem. Soc.* **2005**, *127*, 6819−6829.

(5) Fayette, M.; Nutariya, J.; Vasiljevic, N.; Dimitrov, N. A Study of Pt Dissolution during Formic Acid Oxidation. *ACS Catal.* **2013**, *3*, 1709−1718.

(6) Adzic, R. R.; Zhang, J.; Sazaki, K.; Vukmirovic, M. B.; Shao, M. Platinum Monolayer Fuel Cell Electrocatalysts. *Top. Catal.* **2007**, *46*, 249−262.

DOI: 10.1021/acs.langmuir.5b02351
Langmuir 2015, 31, 10904−10912

(7) van der Vliet, D. F.; Wang, C.; Li, D.; Paulikas, A. P.; Greeley, J.; Rankin, R. B.; Strmcnik, D.; Tripkovic, D.; Markovic, N. M.; Stamenkovic, V. R. Unique Electrochemical Adsorption Properties of Pt-Skin Surfaces. *Angew. Chem., Int. Ed.* **2012**, *51*, 3139−3142.
(8) Greeley, J.; Nørskov, J. K.; Mavrikakis, M. Electronic structure and catalysis on metal surfaces. *Annu. Rev. Phys. Chem.* **2002**, *53*, 319−348.
(9) Hammer, B.; Morikawa, Y.; Nørskov, J. K. CO Chemisorption at Metal Surfaces and Overlayers. *Phys. Rev. Lett.* **1996**, *76*, 2141−2144.
(10) (a) Tyson, W. R.; Miller, W. A. Surface free energies of solid metals: Estimation from liquid surface tension measurements. *Surf. Sci.* **1977**, *62*, 267−276. (b) Kumikov, V. K.; Khokonov, K. B. On the measurement of surface free energy and surface tension of solid metals. *J. Appl. Phys.* **1983**, *54*, 1346−1350.
(11) Alonso, C.; Salvarezza, R. C.; Vara, J. M.; Arvia, A. J.; Vazquez, L.; Bartolome, A.; Baro, A. M. The Evaluation of Surface-Diffusion Coefficients of Gold and Platinum Atoms at Electrochemical Interfaces from Combined STM-SEM Imaging and Electrochemical Techniques. *J. Electrochem. Soc.* **1990**, *137*, 2161−2166.
(12) Waibel, H. F.; Kleinert, M.; Kibler, L. A.; Kolb, D. M. Initial stages of Pt deposition on Au(111) and Au(100). *Electrochim. Acta* **2002**, *47*, 1461−1467.
(13) Sachtler, J. W. A.; Van Hove, M. A.; Bibérian, J. P.; Somorjai, G. A. The structure of epitaxially grown metal films on single crystal surfaces of other metals: Gold on Pt(100) and platinum on Au(100). *Surf. Sci.* **1981**, *110*, 19−42.
(14) Brankovic, S. R.; Wang, J. X.; Adzic, R. R. Metal monolayer deposition by replacement of metal adlayers on electrode surfaces. *Surf. Sci.* **2001**, *474*, L173−L179.
(15) Adzic, R. R.; Zhang, J.; Sasaki, K.; Vukmirovic, M. B.; Shao, M.; Wang, J. X.; Nilekar, A. U.; Mavrikakis, M.; Valerio, J. A.; Uribe, F. Platinum monolayer fuel cell electrocatalysts. *Top. Catal.* **2007**, *46*, 249−262.
(16) (a) Mrozek, M. F.; Xie, Y.; Weaver, M. J. Surface-enhanced Raman scattering on uniform platinum-group overlayers: Preparation by redox replacement of underpotential-deposited metals on gold. *Anal. Chem.* **2001**, *73*, 5953−5960. (b) Rincon, A.; Perez, M. C.; Gutierrez, C. Dependence of low-potential CO electrooxidation on the number of Pt monolayers on gold. *Electrochim. Acta* **2010**, *55*, 3152−3156. (c) Jayaraju, N.; Vairavapandian, D.; Kim, G. Y.; Banga, D.; Stickney, J. L. Electrochemical Atomic Layer Deposition (E-ALD) of Pt Nanofilms Using SLRR Cycles. *J. Electrochem. Soc.* **2012**, *159*, D616−D622.
(17) Fayette, M.; Liu, Y.; Bertrand, D.; Nutariya, J.; Vasiljevic, N.; Dimitrov, N. From Au to Pt via Surface Limited Redox Replacement of Pb UPD in One-Cell Configuration. *Langmuir* **2011**, *27*, 5650−5658.
(18) Vukmirovic, M. B.; Zhang, J.; Sasaki, K.; Nilekar, A. U.; Uribe, F.; Mavrikakis, M.; Adzic, R. R. Platinum monolayer electrocatalysts for oxygen reduction. *Electrochim. Acta* **2007**, *52*, 2257−2263.
(19) Bromberg, L.; Fayette, M.; Martens, B.; Luo, Z. P.; Wang, Y.; Xu, D.; Zhang, J.; Fang, J.; Dimitrov, N. Catalytic Performance Comparison of Shape-Dependent Nanocrystals and Oriented Ultrathin Films of Pt_4Cu Alloy in the Formic Acid Oxidation Process. *Electrocatalysis* **2013**, *4*, 24−36.
(20) (a) Adzic, R. R.; Simic, D. N.; Despic, A. R.; Drazic, D. M. Electrochemical oxidation of formic acid at noble metals: Catalytic effects of foreign metal monolayers. *J. Electroanal. Chem. Interfacial Electrochem.* **1977**, *80*, 81−99. (b) Pletcher, D.; Solis, V. A further investigation of the catalysis by lead ad-atoms of formic acid oxidation at a platinum anode. *J. Electroanal. Chem. Interfacial Electrochem.* **1982**, *131*, 309−323.
(21) Adzic, R. R.; Tripkovic, A. V.; Markovic, N. M. Structural effects in electrocatalysis: Oxidation of formic acid and oxygen reduction on single-crystal electrodes and the effects of foreign metal adatoms. *J. Electroanal. Chem. Interfacial Electrochem.* **1983**, *150*, 79−88.
(22) (a) Hwang, S.-M.; Bonevich, J. E.; Kim, J. J.; Moffat, T. P. Formic Acid Oxidation on $Pt_{100-x}Pb_x$ Thin Films Electrodeposited on Au. *J. Electrochem. Soc.* **2011**, *158*, B1019−B1028. (b) Hwang, S.-M.; Bonevich, J. E.; Kim, J. J.; Moffat, T. P. Electrodeposition of $Pt_{100-x}Pb_x$ Metastable Alloys and Intermetallics. *J. Electrochem. Soc.* **2011**, *158*, D307−D316.
(23) de-los-Santos-Álvarez, N.; Alden, L. R.; Rus, E.; Wang, H.; DiSalvo, F. J.; Abruña, H. D. CO tolerance of ordered intermetallic phases. *J. Electroanal. Chem.* **2009**, *626*, 14−22.
(24) (a) Zhang, L. J.; Wang, Z. Y.; Xia, D. G. Bimetallic PtPb for formic acid electro-oxidation. *J. Alloys Compd.* **2006**, *426*, 268−271. (b) Casado-Rivera, E.; Volpe, D. J.; Alden, L.; Lind, C.; Downie, C.; Vázquez-Alvarez, T.; Angelo, A. C. D.; DiSalvo, F. J.; Abruña, H. D. Electrocatalytic Activity of Ordered Intermetallic Phases for Fuel Cell Applications. *J. Am. Chem. Soc.* **2004**, *126*, 4043−4049.
(25) Kang, Y.; Qi, L.; Li, M.; Diaz, R. E.; Su, D.; Adzic, R. R.; Stach, E.; Li, J.; Murray, C. B. Highly Active Pt_3Pb and Core−Shell Pt_3Pb−Pt Electrocatalysts for Formic Acid Oxidation. *ACS Nano* **2012**, *6*, 2818−2825.
(26) Angerstein-Kozlowska, H.; Conway, B. E.; Hamelin, A.; Stoicoviciu, L. Elementary steps of electrochemical oxidation of single-crystal planes of Au—I. Chemical basis of processes involving geometry of anions and the electrode surfaces. *Electrochim. Acta* **1986**, *31*, 1051−1061.
(27) Trasatti, S.; Petrii, O. A. Real surface area measurements in electrochemistry. *Pure Appl. Chem.* **1991**, *63*, 711−734.
(28) Hamelin, A. Underpotential deposition of lead on single crystal faces of gold - Part 1.The influence of crystallographic oreintation of the substrate. *J. Electroanal. Chem. Interfacial Electrochem.* **1984**, *165*, 167−180.
(29) (a) Shin, J. W.; Bertocci, U.; Stafford, G. R. Stress Responce to Surface Alloying and Dealloying during Underpotential Deposition of Pb on (111) textured Au. *J. Phys. Chem. C* **2010**, *114*, 7926−7932. (b) Nutariya, J.; Velleuer, J.; Schwarzacher, W.; Vasiljevic, N. Surface alloying/dealloying in Pb/Au(111) system. *ECS Trans.* **2010**, *28*, 15−25.
(30) Grgur, B. N.; Markovic, N. M.; Ross, P. N. Underpotential Deposition of Lead on Pt(111) in Perchloric Acid Solution: RRDE Pt(111) Measurements. *Langmuir* **1997**, *13*, 6370−6374.
(31) Clavilier, J.; Orts, J. M.; Gomez, R.; Feliu, J. M.; Aldaz, A. Comparison of electrosorption at activated polycrystalline and Pt(531) kinked platinum electrodes: surface voltammetry and charge displacement on potentiostatic CO adsorption. *J. Electroanal. Chem.* **1996**, *404*, 281−289.
(32) Brankovic, S. R.; Dimitrov, N.; Sieradzki, K. Surfactant Mediated Electrochemical Deposition of Ag on Au(111). *Electrochem. Solid-State Lett.* **1999**, *2*, 443−445.
(33) Popov, A.; Dimitrov, N.; Kashchiev, D.; Vitanov, T.; Budevski, E. A model of the structural transformation process in lead adsorbate on Ag(111) faces at low coverage. *Electrochim. Acta* **1989**, *34*, 269−271.
(34) Vaskevich, A.; Gileadi, E. Underpotential-overpotential transition of a Ag overlayer on Pt: Part3. Influnece of the rearrangment of the overlayer structure on the blocking of hydrogen upd. *J. Electroanal. Chem.* **1998**, *442*, 147−150.
(35) McCall, C.; Dimitrov, N.; Sieradzki, K. Underpotential Deposition on Alloys. *J. Electrochem. Soc.* **2001**, *148*, E290−E293.
(36) Brimaud, S.; Engstfeld, A. K.; Alves, O. B.; Behm, R. J. Structure−reactivity correlation in the oxygen reduction reaction: Activity of structurally well defined $Au_xPt_{1-\xi}$/Pt(111) monolayer surface alloys. *J. Electroanal. Chem.* **2014**, *716*, 71−79.
(37) Kim, J.; Lee, J.; Kim, S.; Kim, Y.-R.; Rhee, C. K. Contrasting Electrochemical Behavior of CO, Hydrogen, and Ethanol on Single-Layered and Multiple-Layered Pt Islands on Au Surfaces. *J. Phys. Chem. C* **2014**, *118*, 24425−24436.
(38) Schulenburg, H.; Durst, J.; Müller, E.; Wokaun, A.; Scherer, G. G. Real surface area measurements of Pt_3Co/C catalysts. *J. Electroanal. Chem.* **2010**, *642*, 52−60.
(39) Parsons, R.; VanderNoot, T. The oxidation of small organic molecules: A survey of recent fuel cell related research. *J. Electroanal. Chem. Interfacial Electrochem.* **1988**, *257*, 9−45.

DOI: 10.1021/acs.langmuir.5b02351
Langmuir 2015, 31, 10904−10912

(40) Wieckowski, A.; Rubel, M.; Gutiérrez, C. Reactive sites in bulk carbon monoxide electro-oxidation on oxide-free platinum(111). *J. Electroanal. Chem.* **1995**, *382*, 97−101.
(41) Caram, J. A.; Gutiérrez, C. An electrochemical and UV-visible potential-modulated reflectance study of the electrooxidation of carbon monoxide on oxide-free smooth platinum: Part 1. Results in 0.5 M $HClO_4$. *J. Electroanal. Chem. Interfacial Electrochem.* **1991**, *305*, 259−274.
(42) Lebedeva, N. P.; Koper, M. T. M.; Feliu, J. M.; van Santen, R. A. The effect of the cooling atmosphere in the preparation of flame-annealed Pt(111) electrodes on CO adlayer oxidation. *Electrochem. Commun.* **2000**, *2*, 487−490.
(43) Lebedeva, N. P.; Koper, M. T. M.; Herrero, E.; Feliu, J. M.; van Santen, R. A. Cooxidation on stepped Pt[n(111)×(111)] electrodes. *J. Electroanal. Chem.* **2000**, *487*, 37−44.
(44) Borup, R. L.; Sauer, D. E.; Stuve, E. M. An ex situ study of electrodeposited lead on platinum (111): I. Examination of the surface redox behavior of lead and dynamic emersion. *Surf. Sci.* **1993**, *293*, 10−26.
(45) Cuesta, A. Measurement of the surface charge density of CO-saturated Pt electrodes as a function of potential: the potential of zero charge of Pt. *Surf. Sci.* **2004**, *572*, 11−22.
(46) (a) Climent, V.; Attard, G. A.; Feliu, J. M. Potential of zero charge of platinum stepped surfaces: a combined approach of CO charge displacement and N_2O reduction. *J. Electroanal. Chem.* **2002**, *532*, 67−74. (b) Attard, G. A.; Ahmadi, A. Anion—surface interactions Part 3. N_2O reduction as a chemical probe of the local potential of zero total charge. *J. Electroanal. Chem.* **1995**, *389*, 175−190.
(47) Trasatti, S. Work function, electronegativity, and electrochemical behaviour of metals: II. Potentials of zero charge and "electrochemical" work functions. *J. Electroanal. Chem. Interfacial Electrochem.* **1971**, *33*, 351−378.
(48) (a) Maillard, F.; Lu, G. Q.; Wieckowski, A.; Stimming, U. Ru-Decorated Pt Surfaces as Model Fuel Cell Electrocatalysts for CO Electrooxidation. *J. Phys. Chem. B* **2005**, *109*, 16230−16243. (b) Gasteiger, H. A.; Markovic, N. M.; Ross, P. N. H_2 and CO Electrooxidation on Well-Characterized Pt, Ru, and Pt-Ru. 1. Rotating Disk Electrode Studies of the Pure Gases Including Temperature Effects. *J. Phys. Chem.* **1995**, *99*, 8290−8301.
(49) Stamenkovic, V. R.; Arenz, M.; Lucas, C. A.; Gallagher, M. E.; Ross, P. N.; Markovic, N. M. Surface Chemistry on Bimetallic Alloy Surfaces: Adsorption of Anions and Oxidation of CO on Pt_3Sn(111). *J. Am. Chem. Soc.* **2003**, *125*, 2736−2745.
(50) Davies, J. C.; Hayden, B. E.; Pegg, D. J.; Rendall, M. E. The electro-oxidation of carbon monoxide on ruthenium modified Pt(1,1,1). *Surf. Sci.* **2002**, *496*, 110−120.
(51) (a) Markovic, N. M.; Schmidt, T. J.; Grgur, B. N.; Gasteiger, H. A.; Behm, R. J.; Ross, P. N. Effect of temperature on surface processes at the Pt(111)-liquid interface: Hydrogen adsorption, oxide formation, and CO oxidation. *J. Phys. Chem. B* **1999**, *103*, 8568−8577. (b) Jusys, Z.; Kaiser, J.; Behm, R. J. Electrooxidation of CO and H_2/CO mixtures on a carbon-supported Pt catalyst-a kinetic and mechanistic study by differential electrochemical mass spectrometry. *Phys. Chem. Chem. Phys.* **2001**, *3*, 4650−4660.
(52) Cuesta, A.; Couto, A.; Rincón, A.; Pérez, M. C.; López-Cudero, A.; Gutiérrez, C. Potential dependence of the saturation CO coverage of Pt electrodes: The origin of the pre-peak in CO-stripping voltammograms. Part 3: Pt(poly). *J. Electroanal. Chem.* **2006**, *586*, 184−195.

DOI: 10.1021/acs.langmuir.5b02351
Langmuir 2015, 31, 10904−10912